Tetrahedron 65 (2009) 4455–4463

Contents lists available at ScienceDirect

Tetrahedron

journal homepage: www.elsevier.com/locate/tet

# Synthesis, characterization, and electroluminescent properties of star shaped donor–acceptor dendrimers with carbazole dendrons as peripheral branches and heterotriangulene as central core

Huaqiang Zhang [a], Shimin Wang [b], Yanqin Li [a], Bin Zhang [b], Chenxia Du [b,*], Xiangjian Wan [a], Yongsheng Chen [a,*]

[a] Key Laboratory for Functional Polymer Materials and Centre for Nanoscale Science and Technology, Institute of Polymer Chemistry, College of Chemistry, Nankai University, 300071 Tianjin, China
[b] Department of Chemistry, Henan Key Laboratory of Chemical Biology and Organic Chemistry, Zhengzhou University, 450052 Zhengzhou, China

ARTICLE INFO

*Article history:*
Received 6 January 2009
Received in revised form 31 March 2009
Accepted 3 April 2009
Available online 9 April 2009

*Keywords:*
Dendrimer
Donor–acceptor (D–A)
Aggregation-induced emission
Organic light emitting diodes (OLEDs)

ABSTRACT

Luminescent and redox-active heterotriangulene-based dendrimers (**G1** and **G2**) of first and second generation have been synthesized, and their photophysical properties, oxidation behaviors, and applications in organic light emitting diodes (OLEDs) have been investigated. The dendrimers show efficient aggregation-induced emissions originated from the carbazole dendrons, heterotriangulene core, intramolecular charge-transfer (ICT), and intermolecular aggregation absorptions. Highest-occupied molecular orbital and lowest-unoccupied molecular orbital (HOMO and LUMO) values were acquired using UV–vis spectroscopy and cyclic voltammetry. The OLEDs fabricated with **G1** and **G2** as non-doping emitters exhibit exclusive aggregation-induced luminescence peaking at 600 and 630 nm, respectively, and demonstrate a good performance with maximum luminance of 1586 cd $m^{-2}$ at current efficiency of 5.3 cd $A^{-1}$ for **G1** and 827 cd $m^{-2}$ at current efficiency of 6.9 cd $A^{-1}$ for **G2**.



## 1. Introduction

In the field of molecular electronics and optoelectronics, various OLEDs based on small molecules and polymers have been extensively studied due to their potential applications in flat-panel or flexible display devices. Dendrimers,[1] as a very special type of polymers with hyperbranched and perfectly defined structure, have attracted much interest for many years. In order to improve the OLED efficiency, periphery to core energy transfer systems based on light harvesting dendrimers have been prepared,[2] which can combine the advantages of small molecules and polymers. The energy transfer occurring in dendrimers can be achieved by a covalently linked donor and acceptor with proper choice of a spacing unit. The rate and efficiency of energy transfer processes can be controlled over factors such as distance and spatial orientation between donor and acceptor.[3] Moreover, incorporation of the electron-transporting moiety (usually acceptor) with the hole-transporting moiety (usually donor) into one dendrimer is expected to balance the carrier-transporting properties of luminophores in dendrimer.[4] In this regard, it is necessary to further study the structure–property relationship of dendrimers containing new donors and acceptors.

Heterotriangulene **A**, based on triphenylamine—a moiety that has been widely exploited for its physical and electronic properties, was first synthesized about 30 years ago.[5,6] Recently, its solid-state structure and photophysical properties were established by Venkataraman et al.[7] The molecule has a planar structure with $D_{3h}$ symmetry and is densely packed into columns in solid state. Its large π-conjugation disc-like structure with three electron-withdrawing carbonyl groups makes itself a good electron-deficient building block for star shaped molecular networks with potential applications for electroluminescent devices.[8] Carbazole is a suitable hole carrier and a promising building block for dendritic construction due to its electronic and optical properties.[9]

By taking advantages of these special properties of **A** and carbazole, we have now synthesized new star shaped dendrimers of the first and second generations incorporating carbazole dendrons as donor branches and **A** as an acceptor core. In this series, we report the synthesis, thermal stability, UV absorption, electrochemical behavior, and the unusual photo- and electroluminescent properties of **G1** and **G2** (Chart 1).

* Corresponding authors. Tel.: +86 22 23500693; fax: +86 22 23499992.
*E-mail addresses:* dcx@zzu.edu.cn (C. Du), yschen99@nankai.edu.cn (Y. Chen).

0040-4020/$ – see front matter © 2009 Elsevier Ltd. All rights reserved.
doi:10.1016/j.tet.2009.04.008

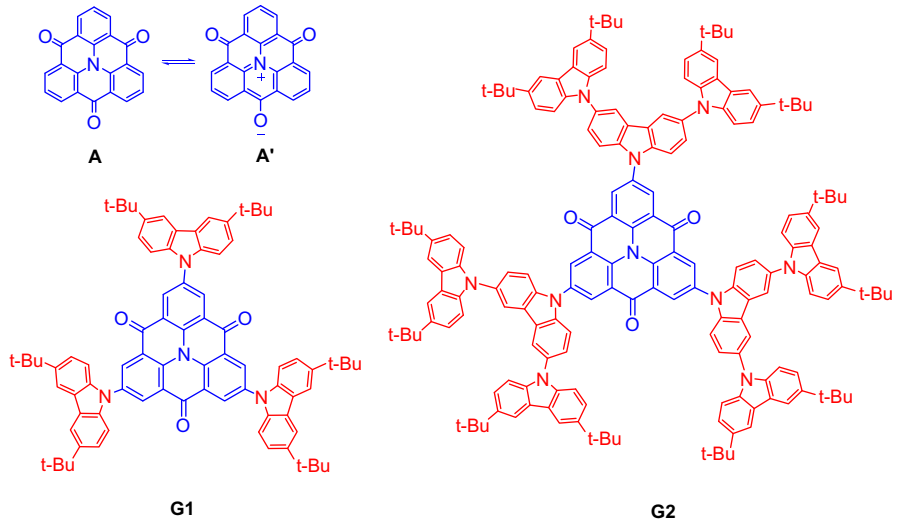


**Chart 1.** Molecular structures of heterotriangulene **A** and its resonance form **A′**, **G1**, and **G2**.

## 2. Results and discussion

### 2.1. Synthesis

The synthesis of the core derivative **3** is outlined in Scheme 1. The starting material **1** was synthesized according to the literature.[7] Compound **2**, obtained using a modified procedure based on literature,[10] was hydrolyzed by potassium hydroxide in the mixture of methanol and water.[11] It was acylated with thionyl chloride and then through an intramolecular Friedel–Crafts reaction to afford **3**.[7] The synthesis of dendrimers **G1** and **G2** is outlined in Scheme 2. **G1** was prepared in two steps, a Friedel–Crafts alkylation of carbazole[12] followed by an Ullmann coupling with **3**.[13] Preparation of **G2** required a multistep process. Tosylation of carbazole and subsequent iodination afforded species **5**.[14] Reaction of **4** and **5** followed by a deprotection of the carbazole nitrogen gave trimer **6**,[15] which was then reacted with **3** to give **G2**.

### 2.2. Thermal analysis

Thermal stabilities of **A**, **G1**, and **G2** were investigated with thermogravimetric analysis (TGA), as shown in Figure 1a. The decomposition temperatures of **G1** and **G2** are about 510 and 490 °C, respectively, which are higher than those of **A** (420 °C). Differential scan calorimetric (DSC) (Fig. 1b) analysis of **A**, **G1**, and **G2** showed no detectable glass transition temperature ($T_g$) or melting temperature ($T_m$) before the decomposition temperature, and therefore they are quite thermally stable and can be used for various high-temperature processes in the construction of electronic devices.

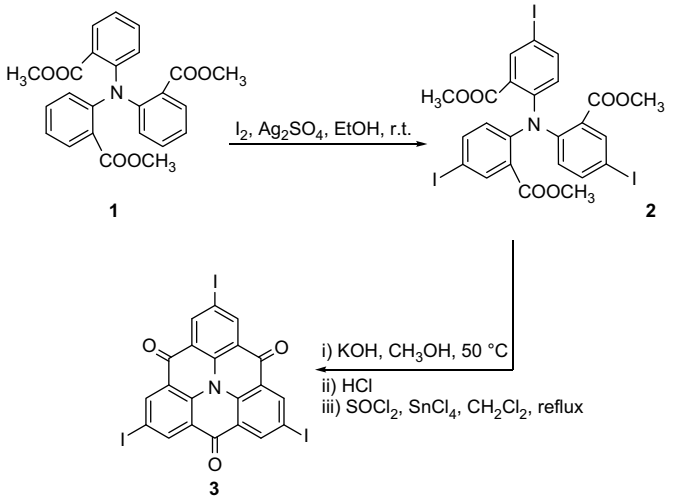


**Scheme 1.** Synthesis of core derivative **3**.

### 2.3. Optical properties

The absorption spectra of **4**, **6**, **G1**, and **G2** in chloroform show intensive transitions in UV region, with strong absorption bands in the range of 200–300 nm (Fig. 2a, Table 1). The bands at about 250 and 296 nm for these compounds are assigned to carbazole centered transitions.[15,16] Overall, the molar absorbance of such bands increases with the number of carbazole units, but not in a manner of good linear relationship. For example, although the molar absorbance of **G1** (containing three carbazole units) is about three times of that of **4**, the molar absorbance of **G2** (containing nine carbazole units) is only about 2.5 times of that of **6** with three carbazole units. While both **6** and **G1** have three carbazole units, the molar absorbance of **G1** is larger than that of **6**. This indicates that the carbazole units in both **G2** and **6** strongly perturb one another.[17]

As indicated by the absorption spectra of **4** and **6**, relatively weak absorption bands are presented at wavelength longer than 300 nm; while the absorption features of **G1** and **G2** at wavelength in 300–370 nm region show moderately strong absorbance (Fig. 2a, Table 1). The band at maximum absorption around 345 nm can be assigned to the transition of the core part (**A**) of **G1** and **G2**, but actually of its resonance form **A′** (Chart 1) according to literature.[5] As already reported for carbazole-phenanthroline compounds,[15] intramolecular charge-transfer (ICT) transitions, in which the **A** core plays the role of acceptor and the carbazole dendrons act as the electron donor, can contribute to the weak bands of **G1** and **G2** at ~370 nm and 420 nm, respectively (inset of Fig. 2a). This is also supported by the solvent dependence of these two bands. For example, the corresponding bands of both **G1** and **G2** appear in dichloromethane and tetrahydrofuran, but disappear in pentane. In addition, the maximum wavelength of ICT transition of **G2** (420 nm) is red-shifted compared to that of **G1** (370 nm), suggesting that the extent of ICT process is more intensified in **G2** than that in **G1**. This is obviously due to the stronger electron donating ability of **6** than that of **4**.[18]

Apart from the characteristic absorptions of the branches and core, the solution spectra of **G1** and **G2** show a new weak broad band

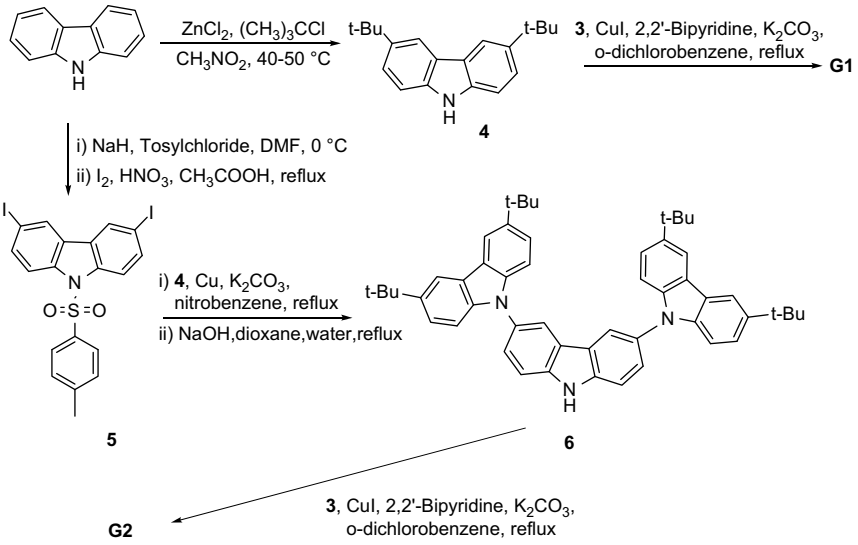


**Scheme 2.** Synthesis of dendrimers **G1** and **G2**.

and a new weak long tail, respectively, at longer wavelength around 500 nm (Fig. 2a and the inset). These absorption features are also presented in the absorption spectra of **G1** and **G2** films on quartz substrate, but more strongly (Fig. 2b). Thus, the absorption features

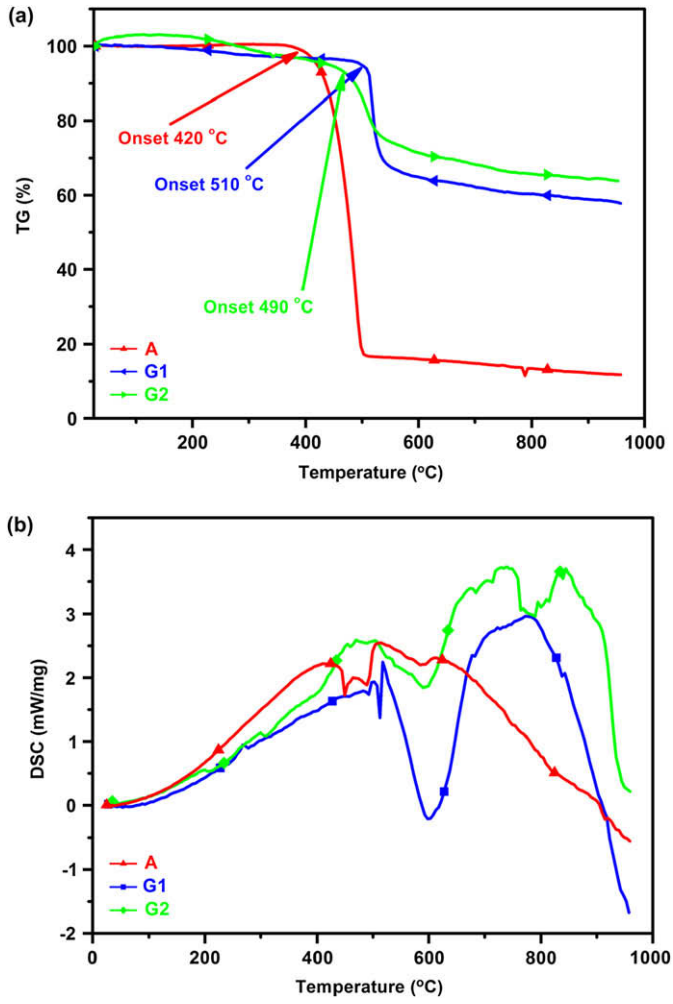


**Figure 1.** TGA (a) and DSC (b) plots of **A**, **G1**, and **G2** with a heating rate of 10 °C min$^{-1}$ under $N_2$ atmosphere.

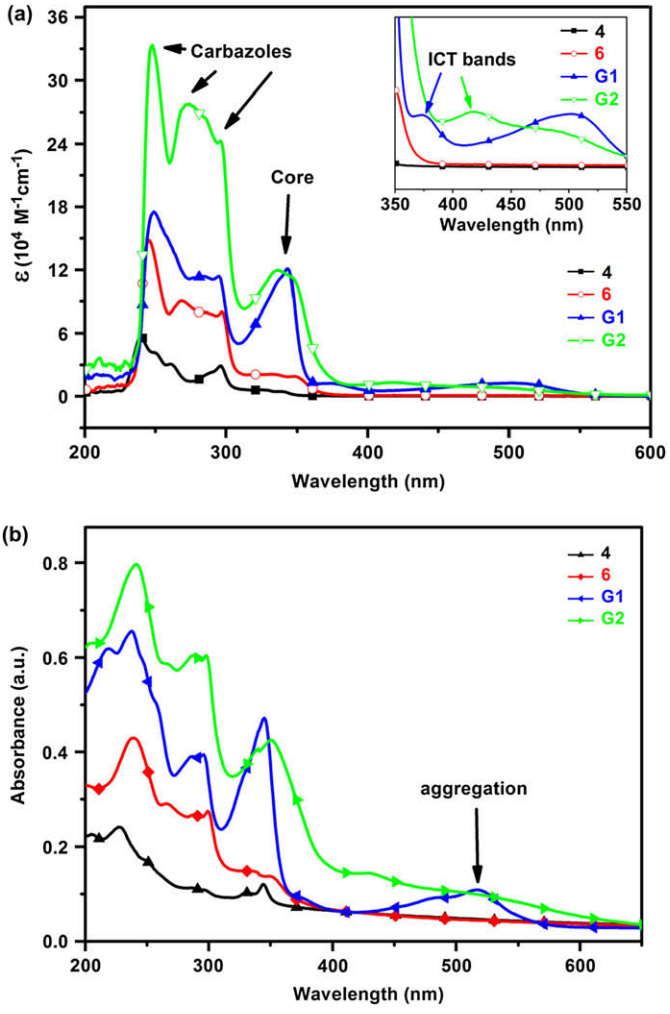


**Figure 2.** Absorption spectra of **4**, **6**, **G1**, and **G2** in degassed chloroform (inset is the amplification of partial spectra) (concentrations **4**: $1.4\times10^{-5}$ M; **6**: $6.0\times10^{-6}$ M; **G1**: $5.0\times10^{-6}$ M; **G2**: $2.4\times10^{-6}$ M, different concentrations were used for an optimal absorbance purpose) (a). Absorption spectra of **4**, **6**, **G1**, and **G2** in thin films spin-coated from chloroform solutions on quartz substrate (b).

**Table 1**
Spectroscopic and photophysical data of **4**, **6**, **G1**, and **G2** in degassed chloroform

| Compound | Absorption | Luminescence | |
|---|---|---|---|
| | $\lambda_{max}$, nm ($\varepsilon$, $M^{-1}\,cm^{-1}$) | $\lambda_{max}$ ($\lambda_{ex}$), nm | $\Phi_{PL}$ |
| **4** | 239 (56 928)<br>295 (29 051)<br>326 (6148) | 363 (296) | 0.536 |
| **6** | 245 (148 196)<br>269 (90 643)<br>297 (80 216)<br>334 (20 913) | 402 (296) | 0.321 |
| **G1** | 250 (175 234)<br>295 (113 978)<br>344 (120 997)<br>370 (12 316) | 430 (350)<br>613 (350, 370, 500)<br>625 (350, 500)[a] | 0.148 |
| **G2** | 250 (333 368)<br>274 (278 046)<br>296 (242 812)<br>337 (119 560)<br>420 (13 065) | 430 (350)<br>650 (350, 500)[a] | 0.077 |

Concentrations **4**: $1.4\times10^{-5}$ M; **6**: $6.0\times10^{-6}$ M; **G1**: $5.0\times10^{-6}$ M; **G2**: $2.4\times10^{-6}$ M.
[a] Data were collected in thin films spin-coated from chloroform solutions on quartz substrate.

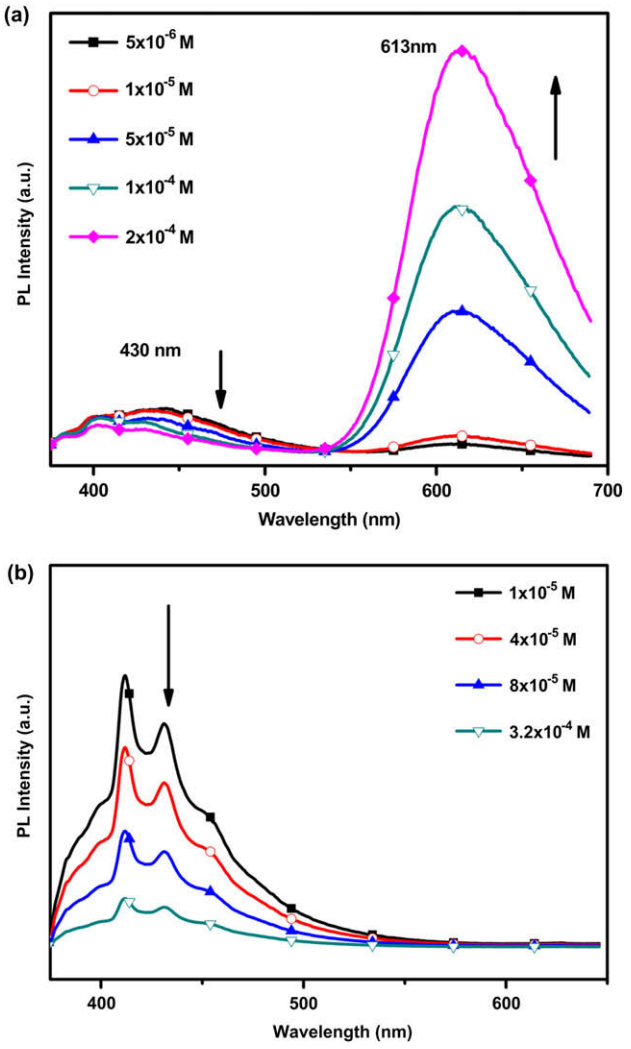


**Figure 3.** Room-temperature uncorrected emission spectra of **G1** (a) and **G2** (b) with different concentrations in degassed chloroform (all excited at 350 nm).

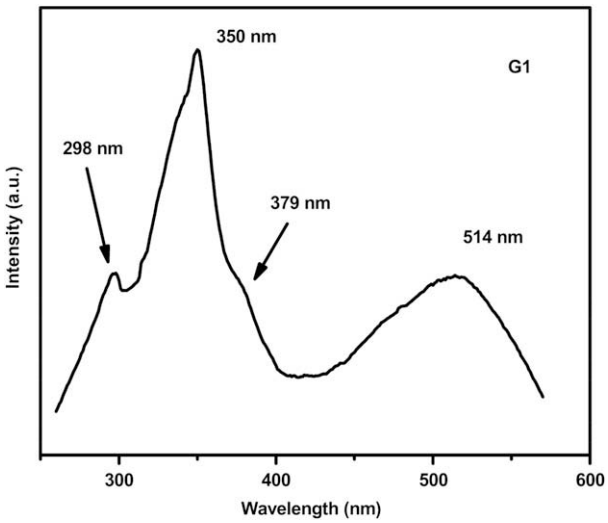


**Figure 4.** Room-temperature uncorrected excitation spectrum of **G1** in degassed chloroform ($\lambda_{em}$=613 nm, the concentration of **G1** is $5.0\times10^{-5}$ M).

of **G1** and **G2** around 500 nm may be attributed to the aggregation formation resulting from the intermolecular interactions between the molecules at high concentrations or neat films.[19]

The photoluminescence (PL) spectra of **G1** and **G2** excited at 350 nm are shown in Figure 3, from which a prominent difference was observed between the two spectra. **G1** and **G2** show the same emission bands around 430 nm. These bands, showing common features of concentration quenching, can be assigned to the emission of the locally excited state of the **A** core.[20] Differently, a very broad featureless emission at 613 nm is observed for **G1**, while no such band could be detected for **G2**. To explore the origin of the band at 613 nm, we measured the fluorescence of **G1** in chloroform with different concentrations. It was found that the emission intensity ratio for band around 430 nm versus band at 613 nm showed apparent concentration dependence. With the increase of concentration of **G1**, the band intensities at 613 nm increase while those around 430 nm show common features of concentration quenching. Considering the bulky dendrons of **G1** and **G2**, these results illustrated that the band of **G1** at 613 nm may originate from the intermolecular J-aggregations where the molecules are arranged in head-to-tail direction rather than the coplanar π–π stacking aggregations.[19,21,22] The absence of this band in **G2** may be

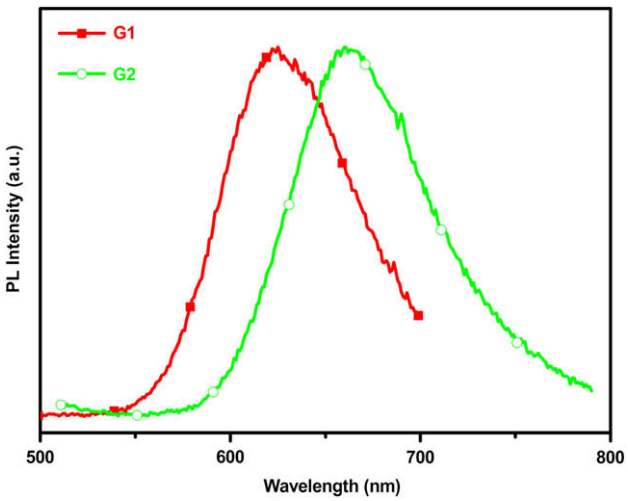


**Figure 5.** Room-temperature corrected emission spectra of **G1** and **G2** (both excited at 500 nm) recorded in thin films spin-coated from chloroform solutions on quartz substrate.

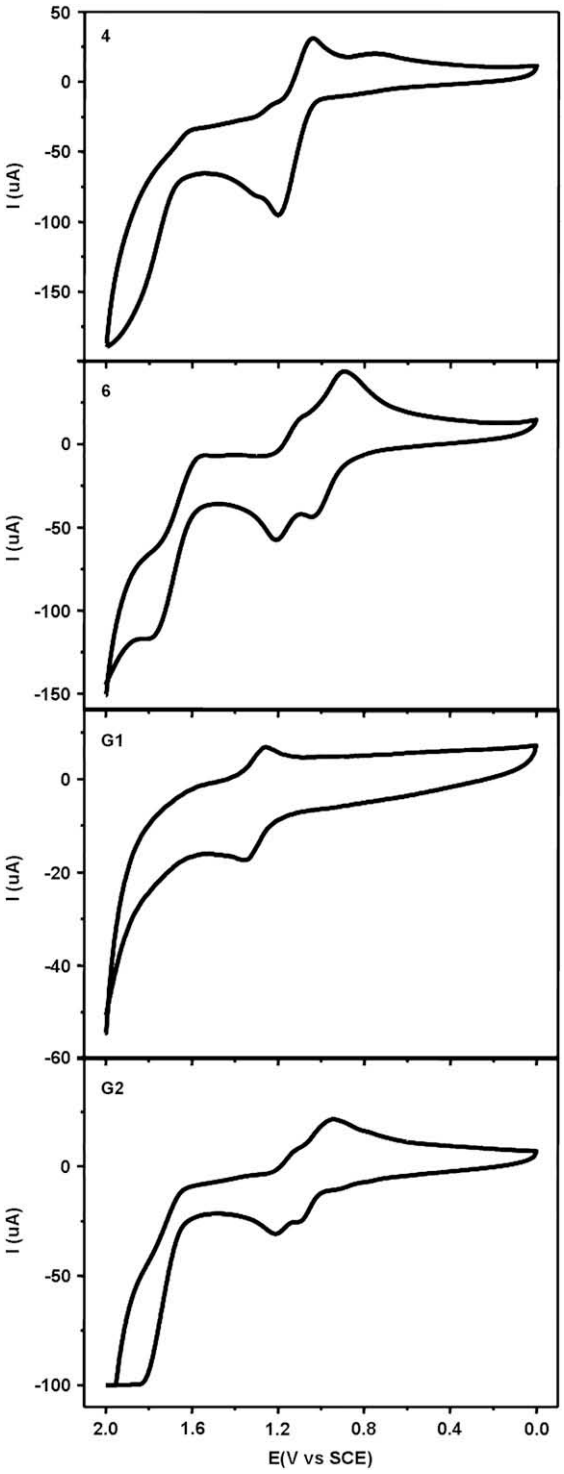


**Figure 6.** Cyclic voltammograms of **4**, **6**, **G1**, and **G2** with the concentration of 0.01 M in 0.1 M $Bu_4NPF_6$–$CHCl_3$, with a glassy carbon electrode at a scan rate of 100 mV $s^{-1}$. A platinum wire and an SCE were used as the counter and reference electrode, respectively.

due to the fact that the more bulky dendrons in **G2** effectively prevent the formation of intermolecular J-aggregation in solution or the more twisted conformations with **G2** in solutions lead to the fast non-radiative relaxation and reduced fluorescence intensity than that of **G1** in solutions.[22,23]

The excitation spectrum of **G1** by monitoring the emission at 613 nm (Fig. 4) provides evidence that the energy absorbed by the carbazole dendrons (298 nm), **A** core (350 nm), ICT (379 nm), and intermolecular J-aggregation (514 nm) can efficiently transfer to the J-aggregation and sensitize the emission at 613 nm. The fluorescence quantum yields ($\Phi_{PL}$) of **4**, **6**, **G1**, and **G2** in dilute solutions in chloroform using quinine sulfate monohydrate as a standard[24] are shown in Table 1.

The thin film emission spectra of **G1** and **G2** excited at 500 nm are shown in Figure 5. The two strong broad and featureless emission bands around 625 and 660 nm can be assigned to the J-aggregation-induced emissions of **G1** and **G2**, where the molecules are arranged in head-to-tail rather than coplanar π–π stacking direction in neat films.[19,21,22] Compared with the fluorescence in solution, the emission band of **G1** in solid film is red-shifted by 12 nm. The red shift can be explained by the fact that in the solid state, the molecules possess a wider distribution of conformations, which gives rise to a lower energy bandgap. When excited at 350 nm, similar PL was observed. This indicates that the excitons produced by direct photoexcitation of the core are likely to migrate readily to the lower energy trapping sites of J-aggregations and sensitize the emissions at 625 and 660 nm, respectively.

**Table 2**
Oxidation potentials of the compounds in degassed chloroform, 298 K

| Compound | $E^{ox}_{1/2}$, V versus SCE |
|---|---|
| **4** | +1.12 [1][a] |
| **6** | +0.97 [1]; +1.16 [1] |
| **G1** | +1.31 [3] |
| **G2** | +1.03 [3]; +1.16 [3] |

[a] The number of exchanged electrons is given in brackets.

## 2.4. Electrochemical properties

Oxidation behavior of **4**, **6**, **G1**, and **G2** has been investigated in chloroform as shown in Figure 6, and the results are summarized in Table 2. It is reported that a carbazole unit can undergo a reversible one-electron oxidation at relatively mild potentials.[15,25] This is consistent with what has been observed for **4**, which undergoes a reversible oxidation process at +1.12 V versus SCE. However, **G1**, with four possible redox centers of three carbazole units and one heterotriangulene core, only undergoes a single reversible oxidation process at +1.31 V versus SCE. Structurally, the three carbazole units in **G1** are separated rather away and independent of each other. So the single reversible oxidation of **G1** can be straightforwardly assigned to simultaneous one-electron oxidation of the three carbazole units as other similar multi-carbazole containing compounds.[17] The oxidation potential of **G1** is anode shifted comparing with that of **4**, which is due to the electron-withdrawing effect of the core in **G1**.

The dendrimer **G2** contains a large number of redox-active centers, including the branches and the core: six outer carbazole units, three inner carbazole units, and one heterotriangulene core. Its dendron subunit, compound **6**, contains three carbazole units with two on outer side and one on inner side. So it is expected that **G2** and **6** would show much richer redox behaviors than **G1** and **4**. But they both undergo only two reversible oxidation processes at

**Table 3**
Electrochemical properties of **4**, **6**, **G1**, and **G2** films

| Compound | $E^{ox}_{onset}$, V versus SCE | $\lambda_{onset}$, nm | $E^{opt}_{g}$,[a] eV | HOMO, eV | LUMO,[b] eV |
|---|---|---|---|---|---|
| **4** | +1.01 | 353 | 3.51 | −5.37 | −1.86 |
| **6** | +0.88 | 380 | 3.26 | −5.24 | −1.98 |
| **G1** | +1.22 | 555 | 2.23 | −5.58 | −3.35 |
| **G2** | +1.01 | 630 | 1.97 | −5.37 | −3.40 |

[a] Estimated from the onset wavelength of optical absorption ($\lambda_{onset}$) in solid-state film.

[b] Calculated using the equation $E_{LUMO}=E_{HOMO}+E^{opt}_{g}$. The reference electrode was calibrated with ferrocene (Fc) and $E_{Fc/Fc+}=0.44$ V versus SCE was used.

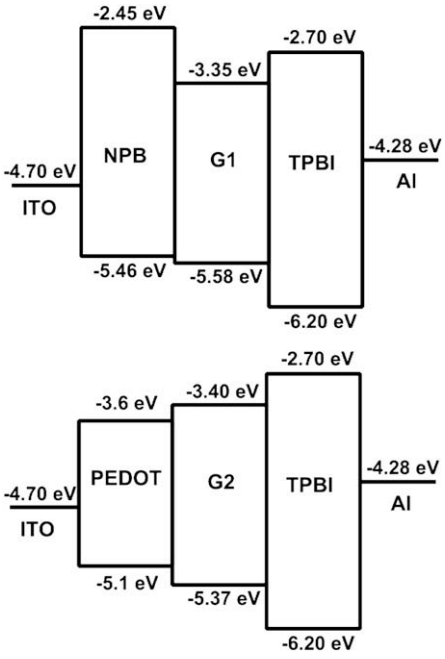


**Figure 7.** The energy level diagram of non-doping OLED with **G1** and **G2** as the emitting layers.

+0.97, +1.16 V for **6** and +1.03, +1.16 V for **G2** versus SCE, respectively. These two compounds are in the series for which the number of reversible oxidation processes is less than the number of carbazole units.[17] Compound **6** undergoes two successive one-electron reversible oxidation processes, separated by 0.19 V. We can assign such processes to successive oxidation of the two outer carbazole units, as observed for the similar compounds reported by Campagna and Dehaen.[15,17] The inner carbazole unit cannot be oxidized within the potential window since its HOMO has already been strongly stabilized due to the directly connected two outer oxidized carbazole units. The separation of the two reversible oxidation processes indicates that significant electronic interaction between the two outer carbazole units takes place in **6** under the experimental condition.[15] Similar results have been observed for the oxidation behavior of **G2**, which undergoes two successive simultaneous three-electron processes, separated by 0.13 V.[17,26] The two successive processes are attributed to the two successive oxidations of the six outer carbazole units. And the three inner carbazole units could not be oxidized within the potential window, as in the case of **6**. Because now the six outer carbazole units have been oxidized into carbazole cations and this makes the HOMO of **G2** strongly stabilized.[17] In contrast to the situation for **G1**, the distance between redox-active carbazole units and the electron-withdrawing core in **G2** is larger, and the HOMO level of **G2** (Table 3) is higher. This explains why the first oxidation potential of **G1** is higher than that of **G2**.

From the thin film absorption spectra (Fig. 2b) and oxidation potentials of **4**, **6**, **G1**, and **G2**, we calculated their absolute values of HOMOs and LUMOs. The HOMO level was obtained from the onset potentials of oxidation by assuming the energy level of ferrocene/ferrocenium ($Fc/Fc^{+}$) to be −4.8 eV below the vacuum level. The LUMO level was calculated from HOMO value and the optical energy gap ($E_g^{opt}$) estimated from the edges of the absorption spectra in films on quartz substrate.[27] Electrochemical data of **4**, **6**, **G1**, and **G2** are summarized in Table 3. The redox behavior of **A** could not be obtained due to its low solubility in suitable organic solvents,[7] therefore its HOMO and LUMO cannot be used for a direct comparison. The HOMO values of **G1** and **G2** are close to those of **4** and **6**, respectively, but slightly negative due to the electron-withdrawing effect of **A** core. The LUMOs of **G1** and **G2** come down significantly, causing a much smaller bandgap of **G1** and **G2** compared to that of **4** and **6**, respectively. These results demonstrate that the HOMOs of **G1** and **G2** should be mainly contributed from the carbazole dendrons and their LUMOs should be mainly contributed from the **A** core. Thus, in these dendrimers, an intramolecular interaction, where **A** acts as an electron-acceptor and carbazole dendrons act as the electron donor, is expected as observed in the UV–vis spectra above.

## 2.5. Electroluminescent (EL) properties

To achieve high performance in organic EL device, it is necessary to attain a hole–electron-transporting balance and effective recombination of holes and electrons in the emitting layer. A three layer device with **G1** was fabricated with the following configuration ITO/NPB (30 nm)/**G1** (20 nm)/TPBI (30 nm)/LiF (1 nm)/Al (100 nm) by a sequential vacuum thermal deposition. Here, **G1** was used as the emitting layer, *N*′(-di-1-naphthyl)-*N*,*N*′-diphenyl-benzidine (NPB) works as the hole-transporting layer, 1,3,5-tris(*N*-phenylbenzimidazol-2-yl)benzene (TPBI) as the hole-blocking and electron-transporting layer. **G2** cannot be vacuum evaporated due to its high molecular weight, a three layer device with **G2** was fabricated using solution process with the following configuration ITO/PEDOT (50 nm)/**G2** (100 nm)/TPBI (30 nm)/LiF (1 nm)/Al (100 nm). A poly(ethylene dioxythiophene) (PEDOT) thin film was deposited on indium tin oxide (ITO) as the anode for facilitating hole injection, and **G2** spin-coated on anode was used both as hole-transporting and emitting layer. A thin film of TPBI with thickness of 30 nm was subsequently vapor deposited on the emitting layer as a hole-blocking and electron-transporting material to confine exciton recombination and limit the loss of the faster moving holes to the cathode. (Details of fabrication for these devices are described in the Experimental section. The structure of devices is illustrated in Fig. 8.)

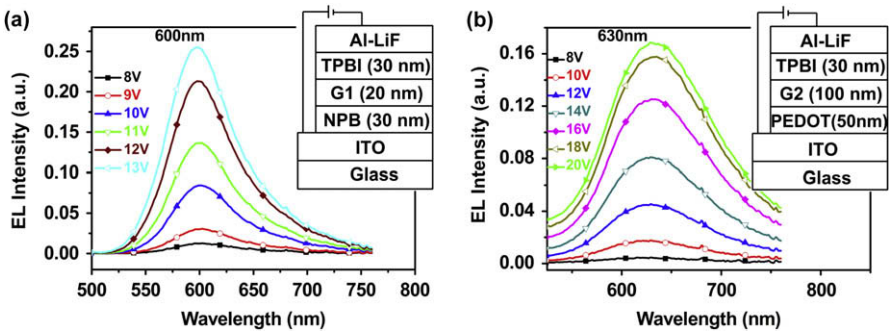


**Figure 8.** EL spectra and cross sections (inset) of the devices with **G1** (a) and **G2** (b).

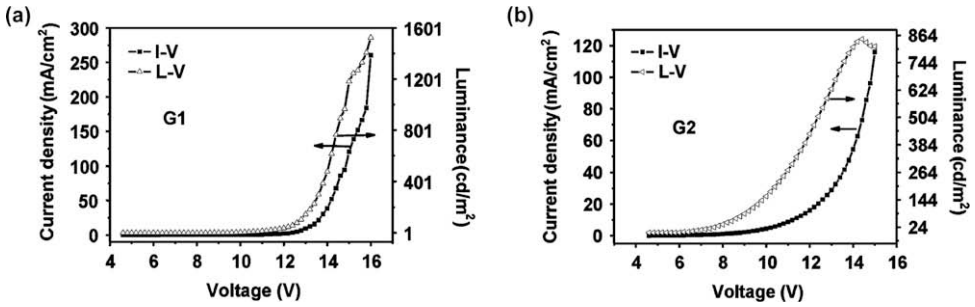


**Figure 9.** Luminance–current density–voltage characteristics of the devices with **G1** (a) and **G2** (b).

The energy level diagrams provide further insight into the roles of main functional materials played in the devices (Fig. 7). In these configurations, holes and electrons are all restricted in the emission layers. For the device with **G1**, the differences in ionization potential ($\Delta I_p$) for ITO/NPB, NPB/**G1** are 0.76, 0.12 eV, and electron affinity ($\Delta E_a$) for Al/TPBI is 1.58 eV, respectively. Also for the device with **G2**, the differences in $\Delta I_p$ for ITO/PEDOT, PEDOT/**G2** are 0.40, 0.27 eV, and $\Delta E_a$ for Al/TPBI is 1.58 eV, respectively. The LUMO levels of **G1** and **G2** are lower than those of TPBI, and therefore there is no electron-injection energy barrier from TPBI to **G1** and **G2**. Although the lower HOMO level of TPBI (−6.20 eV) makes it an efficient hole-blocking layer, but the larger $\Delta E_a$ for Al/TPBI (1.58 eV) will make the electron injection of the device relatively more difficult than those usually observed in ordinary OLEDs with $Alq_3$ as electron-transporting material, indicating possible high turn-on voltages for these devices.[28] Indeed, a high turn-on voltage of 8 V was observed for the both devices with **G1** and **G2**. If an electron-transporting and hole-blocking material with a suitable LUMO level is applied to lower the electron-injection energy barrier, the manipulating voltage would be lowered, and consequently the EL performance would be further improved.

Figure 8 shows the electroluminescence spectra of non-doped devices with **G1** and **G2** as the emission layers. For these two kinds of devices, only red emissions peaking at 600 and 630 nm were observed from **G1** and **G2**, respectively, which closely match the relevant PL spectrum profiles of film samples (Fig. 5). This clearly demonstrates that the emissions from these devices originate from the aggregation-induced emissions of **G1** and **G2**. It should be noted that, compared with the PL spectra of film samples, the EL maximum shows apparent blue shifts of 25 and 30 nm for **G1** and **G2**, respectively. This phenomenon may be attributed to the optical interference of the device structure.[29] Under different applied voltages, the emission spectra are very stable (shown in Fig. 8).

The current–voltage and luminescence–voltage curves of two sets of non-doped devices with **G1** and **G2** are shown in Figure 9. As the voltage increases, the luminescence intensity of **G1** and **G2** increases in exponential manners. For device with **G2**, a maximum luminance of 827 cd $m^{-2}$ at a current density of 120 mA $cm^{-2}$ and a current efficiency of 6.9 cd $A^{-1}$ were acquired at the operation voltage of 14 V. For device with **G1**, a better performance was obtained with a maximum luminescence of 1586 cd $m^{-2}$ at a current density of 296 mA $cm^{-2}$ and a current efficiency of 5.3 cd $A^{-1}$, when operated at the voltage of 16 V. Furthermore, the current efficiencies decay gently with increasing current densities especially for OLED with **G2**. Although neither the configurational nor the compositional structure of the present devices is optimized, the two OLEDs show good EL performances compared with those of other dendrimers.[30] It is especially interesting to note that there is almost no concentration quenching in OLEDs based on non-doping **G1** and **G2** owing to their aggregation-induced emission properties. This implies that **G1** and **G2** are good candidates for efficient non-doped red OLEDs.

## 3. Conclusions

In summary, we have synthesized two star shaped donor–acceptor dendrimers with carbazole branches and heterotriangulene core using Cu-catalyzed Ullmann coupling reaction and these two compounds show good thermal stabilities. The dendrimers show distinct ground state intramolecular charge-transfer (ICT) transitions between carbazole branches and heterotriangulene core as confirmed by UV–vis spectra and cyclic voltammetric studies. The relative smaller band gaps and the energies of their HOMOs and LUMOs suggest that the dendrimers favor transport of both holes and electrons. The photoluminescence of dendrimers at room temperature shows the characteristics of locally excited emissions in diluted solutions, while aggregation-induced emissions in thin films. The electroluminescent devices with **G1** and **G2** as non-doping emitters show good EL performances. And there is almost no concentration quenching in OLEDs based on non-doping **G1** and **G2** owing to their aggregation-induced emission properties. Intensive studies on electroluminescent properties by modifications of donors or acceptors to the structures of these derivative materials are in progress.

## 4. Experimental

### 4.1. General materials and methods

Unless stated otherwise, all chemicals and reagents were purchased reagent-grade and used without further purification. Solvents were purified by standard methods. All manipulations were performed under a dry argon atmosphere using standard Schlenk techniques. *N*,*N*′(-Di-1-naphthyl)-*N*,*N*′-diphenyl-benzidine (NPB), and 1,3,5-tris(*N*-phenylbenzimidazol-2-yl)benzene (TPBI) were purified by sublimation prior to use.

$^1$H NMR and $^{13}$C NMR spectra were recorded on a Bruker AC-300 Spectrometer. Chemical shifts, $\delta$, were reported in parts per million relative to the internal standard TMS. Mass spectra (MS) were recorded using an LCQ Advantage mass spectrometer. High resolution mass spectra (HRMS) were recorded on a VG ZAB-HS mass spectrometer. FTIR spectra were recorded on Bruker-Tensor 27 spectrometer. Elemental analyses were measured using a Yanaca CDRDER MT-3 instrument. Thermogravimetric analysis (TGA) measurement was performed on a TA instrument SDT-TG Q600 under an atmosphere of $N_2$ at a heating rate of 10 °C $min^{-1}$. Differential scanning calorimetric (DSC) measurement was recorded on a TA instrument DSC-2910, under an atmosphere of $N_2$ at a heating rate of 10 °C $min^{-1}$. UV spectra were recorded on a JASCO-V570 spectrometer. Cyclic voltammetry (CV) measurement was performed on an LK98B II Microcomputer-based Electrochemical Analyzer at room temperature with a three-electrode cell in a solution of $Bu_4NPF_6$ (0.1 M) in chloroform at a scanning rate of 100 mV $s^{-1}$. A platinum wire was used as a counter electrode, and an SCE electrode was used as a reference electrode. After

measurement the reference electrode was calibrated with ferrocene (Fc). For steady state luminescence measurements, a JOBIN YVON HORIBA spectrometer was used. Luminescence quantum yields have been calculated by the optically diluted method.[24]

*Fabrication of OLED for* ***G1***: ITO coated glass with a sheet resistance of 20 Ω square$^{-1}$ was used as substrate and anode. Before loading into a deposition chamber, the ITO coated glass was washed with organic solvents, deionized water and finally treated with ultraviolet (UV)–ozone. The organic and metal layers were all deposited in the same vacuum chamber with a base pressure better than $3\times10^{-4}$ Pa without any vacuum break-in among the different deposition processes. *The fabrication of OLED for* ***G2*** is prepared according to the following standard procedure: ITO coated glass substrates were cleaned via repeated ultrasonic washing and oxygen plasma treating. The buffer layer was spin-coated from the aqueous dispersion of PEDOT. The active dendrimer layer of **G2** was spin-coated from 1.2 wt % toluene/chloroform solution. The cathode layer LiF (1 nm)/Al (100 nm) for OLEDs with **G1** and **G2** was finally deposited on the organic layers under the same condition. The thickness of the evaporated layers was monitored by an in-situ quartz crystal microbalance. EL spectra and luminance–current–voltage characteristics of the devices were measured with a computer controlled source meter Keithley 236 spectrograph. All device tests were carried out under an ambient atmosphere at room temperature.

## 4.2. Synthesis of compounds

*O*,*O*′,*O*″-Amino-trisbenzoic acid-trimethylester[9] (**1**), 3,6-di-*tert*-butyl-9*H*-carbazole[14] (**4**), 3,6-diiodo-9-(toluene-4-sulfonyl)carbazole[16] (**5**), and 3,6,3″,6″-tetrakis-*tert*-butyl-9′*H*-[9,3′;6′,9″]tercarbazole[17] (**6**) were prepared according to previously reported procedures and showed identical spectroscopic properties to those reported therein.

### 4.2.1. *O*,*O*′,*O*″-Amino-tris 4-iodobenzoic acid-trimethylester (*2*)

*O*,*O*′,*O*″-Amino-trisbenzoic acid-trimethylester (**1**) (1.00 g, 2.39 mmol) was added to a mixture of iodine (1.80 g, 2.39×3 mmol) and silver sulfate (2.23 g, 2.39×3 mmol) in ethanol (150 mL) at room temperature. The mixture was stirred for 12 h. The solid was removed by filtration through a thin pad of silica gel and the filtrate was evaporated to dryness under reduced pressure to give a yellow powder (1.71 g, yield 90%). The residue was used without further purification. Mp 163–165 °C; $^1$H NMR (300 MHz, $CDCl_3$, ppm) $\delta$ 7.911 (d, $^4J$=2.1 Hz, 1H), 7.648 (dd, $^3J$=8.6 Hz, $^4J$=2.1 Hz, 1H), 6.772 (d, $^3J$=8.6 Hz, 1H), 3.434 (s, 3H); MS (ESI) *m*/*z* 820.1 ($M+Na^+$).

### 4.2.2. Triketone (*3*)

*O*,*O*′,*O*″-Amino-tris 4-iodobenzoic acid-trimethylester (**2**) (3.00 g, 3.76 mmol), potassium hydroxide (3.22 g, 3.76×15 mmol), methanol (200 mL), and water (50 mL) were added to a 500 mL flask. The mixture was stirred overnight at 50 °C, and then cooled, diluted with 1000 mL water, and acidified with 1 M hydrochloric acid to pH ~ 3. The precipitate was isolated by filtration and dried under vacuum to give a pale solid (2.70 g, yield 95%) and used without further purification for next step. This pale solid (tri-acid intermediate) (1.50 g, 1.99 mmol), $SOCl_2$ (4.40 mL, 1.99×30 mmol), and DMF (0.5 mL) were refluxed in dry dichloromethane (50 mL) for 3 h. $SnCl_4$ (4.2 mL, 1.99×18 mmol) was then added and the reaction was refluxed for an additional 24 h. The mixture was cooled a little and filtered to collect the yellow solid product. The product was added to a stirred solution of aqueous sodium hydroxide and stirred for 1 h. The precipitate was collected by filtration and washed with water, acetone and then dried to give the title compound as a yellow solid (0.70 g, yield 50%). The triketone (**3**) was characterized by IR due to its low solubility in common organic solvent. Mp >300 °C; IR (KBr) $\nu$=3057, 1653, 1593, 1439, 1319, 1279, 800, 717 cm$^{-1}$.

### 4.2.3. G1

A mixture of 3,6-di(*tert*-butyl)carbazole (**4**) (0.32 g, 0.286×4 mmol), copper(I) iodide (0.033 g, 0.286×0.2×3 mmol), 2,2′-bipyridine (0.027 g, 0.286×0.2×3 mmol), potassium carbonate (0.40 g, 0.286×10 mmol), and **3** (0.20 g, 0.286 mmol) were refluxed in *o*-dichlorobenzene (30 mL) for 24 h. After the mixture was cooled to room temperature, dichloromethane was added and the mixture was filtered. The filtrate was condensed under reduced pressure, and the residue was purified by chromatography on silica gel with a mixture of petroleum ether/dichloromethane (3:1, v/v) as eluent. The **G1** product was obtained as a red solid (0.28 g, yield 85%). Mp >300 °C; $^1$H NMR (300 MHz, $CDCl_3$, ppm) $\delta$ 9.338 (s, 2H), 8.206 (s, 2H), 7.586 (d, $^3J$=8.7 Hz, 2H), 7.544 (dd, $^3J$=8.7 Hz, $^4J$=1.5 Hz, 2H), 1.501 (s, 18H); $^{13}$C NMR (75 MHz, $CDCl_3$, ppm) $\delta$ 175.5, 144.6, 138.7, 137.1, 135.5, 131.7, 125.2, 124.5, 116.9, 108.9, 35.1, 32.2; HRMS (MALDI) *m*/*z* 1155.7690 ($C_{81}H_{79}N_4O_3$ $[M+H]^+$ requires 1155.6152); IR (KBr) $\nu$=2961, 1659, 1475, 1296, 804, 608 cm$^{-1}$. Elemental analysis calcd for $C_{81}H_{78}N_4O_3$: C, 84.19; H, 6.80; N, 4.85%. Found: C, 84.12; H, 6.86; N, 4.90%.

### 4.2.4. G2

A mixture of 3,6,3″,6″-tetrakis-*tert*-butyl-9′*H*-[9,3′;6′,9″]-tercarbazole (**6**) (0.83 g, 0.286×4 mmol), copper(I) iodide (0.033 g, 0.286×0.2×3 mmol), 2,2′-bipyridine (0.027 g, 0.286×0.2×3 mmol), potassium carbonate (0.40 g, 0.286×10 mmol), and **3** (0.20 g, 0.286 mmol) were refluxed in *o*-dichlorobenzene (25 mL) for 36 h. After the mixture was cooled to room temperature, dichloromethane was added and the mixture was filtered. The filtrate was condensed under reduced pressure, and the residue was purified by chromatography on silica gel with a mixture of petroleum ether/dichloromethane (2:1, v/v) as eluent. The **G2** product was obtained as a deep brown solid (0.57 g, yield 80%). Mp >300 °C; $^1$H NMR (300 MHz, $CDCl_3$, ppm) $\delta$ 9.577 (s, 2H), 8.338 (d, $^3J$=1.8 Hz, 2H), 8.175 (d, $^4J$=1.6 Hz, 4H), 7.852 (d, $^3J$=8.7 Hz, 2H), 7.735 (dd, $^3J$=8.7 Hz, $^4J$=1.8 Hz, 2H), 7.493 (dd, $^3J$=8.7 Hz, $^4J$=1.6 Hz, 4H), 7.393 (d, $^3J$=8.6 Hz, 4H), 1.473 (s, 36H); $^{13}$C NMR (75 MHz, $CDCl_3$, ppm) $\delta$ 175.4, 143.1, 140.2, 139.9, 136.5, 132.7, 132.6, 126.8, 125.7, 125.2, 123.9, 123.5, 119.9, 116.5, 110.8, 109.3, 35.0, 32.3; HRMS (MALDI) *m*/*z* 2482.7807 ($C_{177}H_{169}N_{10}O_3$ $[M+H]^+$ requires 2482.3379); IR (KBr) $\nu$=2957, 1724, 1661, 1470, 1364, 1283, 806, 609 cm$^{-1}$. Elemental analysis calcd for $C_{177}H_{168}N_{10}O_3$: C, 85.61; H, 6.82; N, 5.64%. Found: C, 85.55; H, 6.88; N, 5.72%.

## Acknowledgements

We gratefully acknowledge the financial support from the NSFC (#20774047), MoST (#2006CB932702), and NSF of Tianjin City (#07JCYBJC03000, #08JCZDJC25300).

## References and notes

1. Majoral, J. P.; Caminade, A. M. *Chem. Rev.* **1999**, *99*, 845.
2. (a) Kwok, C. C.; Wong, M. S. *Chem. Mater.* **2002**, *14*, 3158; (b) Weil, T.; Reuther, E.; Müllen, K. *Angew. Chem., Int. Ed.* **2002**, *41*, 1900; (c) Adronov, A.; Malenfant, P. R. L.; Fréchet, J. M. J. *Chem. Mater.* **2000**, *12*, 1463; (d) Furuta, P.; Brooks, J.; Thompson, M. E.; Fréchet, J. M. J. *J. Am. Chem. Soc.* **2003**, *125*, 13165; (e) Furuta, P.; Fréchet, J. M. J. *J. Am. Chem. Soc.* **2003**, *125*, 13173.
3. (a) Saha, D. C.; Bhattacharjee, D.; Misra, T. N. *Opt. Mater.* **1998**, *10*, 285; (b) Kuragaki, M.; Sisido, M. *J. Phys. Chem.* **1996**, *100*, 16019.
4. Kwok, C. C.; Wong, M. S. *Macromolecules* **2001**, *34*, 6821.
5. Hellwinkel, D.; Melan, D. *Chem. Ber.* **1971**, *104*, 1001.
6. Hellwinkel, D.; Melan, M. *Chem. Ber.* **1974**, *107*, 616.
7. Field, J. E.; Venkataraman, D. *Chem. Mater.* **2002**, *14*, 962.
8. Amir, P.; Horst, V.; Susanne, H.; Holger, H.; Philipp, S.; Rocco, F. WO 2007/031165, 2007.

9. (a) Ding, J. Q.; Gao, J.; Cheng, Y. X.; Xie, Z. Y.; Wang, L. X.; Ma, D. G.; Jing, X. B.; Wang, F. S. *Adv. Funct. Mater.* **2006**, *16*, 575; (b) Burn, P. L.; Lo, S. C.; Samuel, I. D. W. *Adv. Mater.* **2007**, *19*, 1675; (c) Albrecht, K.; Kasai, Y.; Kimoto, A.; Yamamoto, K. *Macromolecules* **2008**, *41*, 3793; (d) Bolink, H. J.; Santamaria, S. G.; Sudhakar, S.; Zhen, C. G.; Sellinger, A. *Chem. Commun.* **2008**, 618; (e) Lin, Y. H.; Wu, H. H.; Wong, K. T.; Hsieh, C. C.; Lin, Y. C.; Chou, P. T. *Org. Lett.* **2008**, *10*, 3211.
10. Sy, W. W. *Synth. Commun.* **1992**, *22*, 3215.
11. Slutsky, M. M.; Jones, T. V.; Tew, G. N. *J. Org. Chem.* **2007**, *72*, 342.
12. Liu, Y.; Nishiura, M.; Wang, Y.; Hou, Z. M. *J. Am. Chem. Soc.* **2006**, *128*, 5592.
13. Kelkar, A. A.; Patil, N. M.; Chaudhari, R. V. *Tetrahedron Lett.* **2002**, *43*, 7143.
14. Tucker, S. H. *J. Chem. Soc.* **1926**, 546.
15. McClenaghan, N. D.; Passalacqua, R.; Loiseau, F.; Campagna, S.; Verheyde, B.; Hameurlaine, A.; Dehaen, W. *J. Am. Chem. Soc.* **2003**, *125*, 5356.
16. Bigelow, R. W.; Johnson, G. E. *J. Chem. Phys.* **1977**, *66*, 4861.
17. Loiseau, F.; Campagna, S.; Hameurlaine, A.; Dehaen, W. *J. Am. Chem. Soc.* **2005**, *127*, 11352.
18. Sumalekshmy, S.; Gopidas, K. R. *Photochem. Photobiol. Sci.* **2005**, *4*, 539.
19. An, B. K.; Kwon, S. K.; Jung, S. D.; Park, S. Y. *J. Am. Chem. Soc.* **2002**, *124*, 14410.
20. Rajendiran, N.; Sivakumar, K.; Stalin, T. *Spectrochim. Acta, Part A* **2005**, *62*, 991.
21. Gruszecki, W. I. *J. Biol. Phys.* **1991**, *18*, 99.
22. Oelkrug, D.; Tompert, A.; Gierschner, J.; Egelhaaf, H. J.; Hanack, M.; Hohloch, M.; Steinhuber, E. *J. Phys. Chem. B* **1998**, *102*, 1902.
23. (a) Oelkrug, D.; Tompert, A.; Egelhaaf, H.; Hanack, M.; Steinhuber, E.; Hohloch, M.; Meier, H.; Stalmach, U. *Synth. Met.* **1996**, *83*, 231; (b) Souza, M. M.; Rumbles, G.; Gould, I. R.; Amer, H.; Samuel, I. D. W.; Moratti, S. C.; Holmes, A. B. *Synth. Met.* **2000**, *111–112*, 539.
24. Demas, J. N.; Crosby, G. A. *J. Phys. Chem.* **1971**, *75*, 991.
25. Kido, J.; Hongawa, K.; Okuyama, K.; Nagai, K. *Appl. Phys. Lett.* **1993**, *63*, 2627.
26. Flanagan, J. B.; Margel, S.; Bard, A. J.; Anson, F. C. *J. Am. Chem. Soc.* **1978**, *100*, 4248.
27. (a) Li, J. Y.; Ma, C. W.; Tang, J. X.; Lee, C. S.; Lee, S. T. *Chem. Mater.* **2005**, *17*, 615; (b) Ma, Z.; Lu, S.; Fan, Q. L.; Qing, C. Y.; Wang, Y. Y.; Wang, P.; Huang, W. *Polymer* **2006**, *47*, 7382.
28. Zhang, Z.; Liu, X. D.; Li, Z. Y.; Chen, Z. H.; Zhao, F. Q.; Zhang, F. S.; Tung, C. H. *Adv. Funct. Mater.* **2008**, *18*, 302.
29. (a) Cimrova, V.; Neher, D. *J. Appl. Phys.* **1996**, *79*, 3299; (b) Leger, J. M.; Carter, S. A.; Ruhstaller, B.; Nothofer, H. G.; Scherf, U.; Tillman, H.; Horhold, H. H. *Phys. Rev. B* **2003**, *68*, 054209; (c) Qiu, Y.; Wei, P.; Zhang, D. Q.; Qiao, J.; Duan, L.; Li, Y. K.; Gao, Y. D.; Wang, L. D. *Adv. Mater.* **2006**, *18*, 1607.
30. (a) Liu, Q. D.; Lu, J. P.; Ding, J. F.; Day, M.; Tao, Y.; Barrios, P.; Stupak, J.; Chan, K.; Li, J. J.; Chi, Y. *Adv. Funct. Mater.* **2007**, *17*, 1028; (b) Sun, X. B.; Xu, X. J.; Qiu, W. F.; Yu, G.; Zhang, H. J.; Gao, X. K.; Chen, S. Y.; Song, Y. L.; Liu, Y. Q. *J. Mater. Chem.* **2008**, *18*, 2709.